JOURNAL OF SOLID STATE CHEMISTRY 117, 108–121 (1995)

Fast-Ion Conducting $Y_2(Zr_yTi_{1-y})_2O_7$ Pyrochlores: Neutron Rietveld Analysis of Disorder Induced by Zr Substitution

Catherine Heremans and Bernhardt J. Wuensch

Department of Materials Science and Engineering, Massachusetts Institute of Technology, Cambridge, Massachusetts 02139

and

Judith K. Stalick and Edward Prince

Reactor Radiation Division, National Institute of Standards and Technology, Gaithersburg, Maryland 20899

Received July 25, 1994; accepted November 28, 1994

The structure of $Y_2(Zr_yTi_{1-y})_2O_7$ solid solutions progressively changes, with increasing y, from an ordered pyrochlore structure $A_2B_2O_7\square$, space group $Fd3m$, to a deflect-fluorite structure $(A, B)_4$ $(O_{0.875}\square_{0.125})_8$, space group $Fm3m$, at $y = 0.90$. The anion array consists of three independent sites O(1), O(2), and O(3), occupying positions 48f, 8a and 8b, respectively, of which 8b is unoccupied in a fully ordered pyrochlore. Rietveld powder-profile analysis of data collected with 1.5453-Å thermal neutrons was used to determine the structural state of four samples with increasing Zr content ($y = 0.30$, 0.45, 0.60, and 0.90). Refinements that employed only the pyrochlore superstructure intensity data provided weighted profile residuals that ranged 8.06 to 8.67% compared with expected values of 7.13 to 7.87% derived from counting statistics. The onset of disorder at $y = 0.30$ is marked by filling of the vacant 8b site with oxygen ions displaced from the nearest-neighbor anion shell—i.e., O(1) in 48f. Only for $y > 0.45$ does O(2) participate in the disorder. Mixing of the occupancy of cation sites A and B begins only with under occupancy of the O(2) site. The eight-coordinated A site, position 16c, is occupied solely by Y for $y \leq 0.45$ and is predominantly Y at $y = 0.60$. The substituted Zr^{4+} thus replaces Ti^{4+} in the six-coordinated B site for most of the solid–solution series. Complete mixing of all three cation species occurs abruptly over the narrow compositional range $0.60 < y \leq 0.90$. The disordered structural states cannot be described by a single-order parameter. The O(1) ion is displaced 0.46 Å toward the vacant O(3) site in the ordered pyrochlore at $y = 0$. The displacement relaxes to the ideal position of the fluorite structure with a quadratic dependence on y. Increase of the anisotropic temperature-factor coefficients with y indicates general softening of the structure with increased disorder. The array of O(1) ions forms a continuous path for migration of anions through the structure. The magnitude and composition dependence of the reported change of ionic conductivity with y may be satisfactorily explained by the variation of the product of charge-carrier concentration and vacancy concentration $N(N - 1)$, where N is taken as the site occupancy of O(1). © 1995 Academic Press, Inc.

INTRODUCTION

Phases of general formula $A_2B_2O_7$ with the pyrochlore structure are cubic superstructures with lattice constant twice that of a fluorite-like array of parent atoms. Figure 1 shows a projection along a_3 of the cell contents for $0 \leq z \leq 1/4$. A large trivalent A cation and a smaller quadrivalent B cation order in alternating ⟨110⟩ rows and respectively occupy positions 16c and 16d of space group $Fd3m$. The seven oxygen ions per unit formula define three different sites that are directly related to the eight anion sites in the fluorite substructure. Six oxygen ions per fluorite subcell occupy position 48f, x 1/8 1/8. These ions, designated O(1), have positional parameter $x \geq 3/8$ and thus display relaxation toward a vacant site at position 8b, 3/8 3/8 3/8, that is normally occupied in the fluorite structure. The second type of anion, O(2), occupies position 8a, 1/8 1/8 1/8.

Progressive structural disorder takes place in pyrochlore solid solutions as the average radii of the A and B cations become similar. A defective fluorite-like structure $MO_{1.75}$ is attained at complete disorder. Analogously, for a given radius ratio of the two cations, there exists a transition temperature above which the defect fluorite structure is preferred over the pyrochlore structure. Different explanations have emerged for these disordering phenomena in the zirconates and titanates of the lanthanide elements. A first model proposed short-range disorder at the atomic scale: on the cation sites, on the anion sites, or simultaneously on both (1–7). General dsorder results from progressive mixing of the occupancies of these sites. In a second model, regions of ordered pyrochlore were believed to coexist with regions with disordered fluorite-like structure; both coherent (5) and incoherent (8) interfaces between such regions have been proposed. A third

0022-4596/95 $6.00
Copyright © 1995 by Academic Press, Inc.
All rights of reproduction in any form reserved.

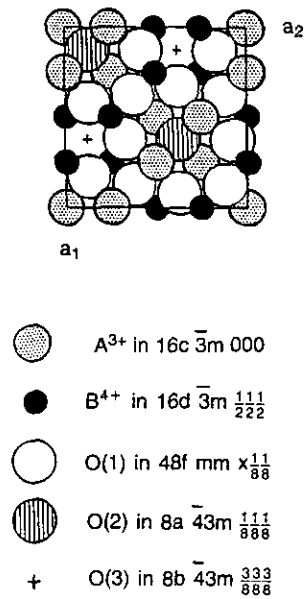

FIG. 1. Projection of the contents of the pyrochlore supercell for $0 \le z \le \frac{1}{4}$. The O(1) locations are those found for $Y_2Ti_2O_7$ and show a displacement of 0.46 Å toward the O(3) position, a site that is unoccupied in a fully ordered pyrochlore structure.

interpretation (9–12) suggests the presence of antiphase boundaries between pyrochlore domains. The size of the antiphase domains seemed strongly correlated with the radius ratio of the cations and the transition temperature. In the last model, imperfectly ordered pyrochlore regions might have grown larger at the expense of the fluorite phase and impinged to form antiphase boundaries.

The electrical conductivity of various pyrochlore phases and their solid solutions has been measured (13–15), including those in the Y_2 $(Zr_yTi_{1-y})_2$ O_7 system (6, 16, 17). As the Ti cation is replaced by the larger Zr cation or, equivalently, as the ratio of the average radii of cations *A* and *B* decreases, the solid solution disorders completely to the defect fluorite structure. A remarkable increase in conductivity by three orders of magnitude (for example, to 10^{-2} S cm^{-1} at 1000°C) accompanies the disorder (16).

Neutron powder diffraction methods were used in the present work to determine the state of structural disorder in yttrium titanate–yttrium zirconate solid solutions as a function of composition. A preliminary account of some early results has appeared elsewhere (18). Our objective was to provide insight into the mechanism by which the conductivity is enhanced. As both the anion and cation arrays display no long-range order in compositions with high Zr content, a particularly interesting question is whether disorder in the anion and cation arrays progresses at different rates with increasing *y* or whether the processes are coupled; in other words, whether the structure can be described with a single order parameter or whether more than one is required.

EXPERIMENTAL

Powders of compositions with $y = 0.30$, 0.45, 0.60, and 0.90 were prepared by the Pechini process (19). This chemical method is based on the dissolution of metal compounds (Y hydroxide, Ti and Zr alkoxides in the present work) in a mixture of citric acid and ethylene. A mixture of solutions in appropriate proportions was polymerized in a first heating step. The organic constituents were then charred, followed by calcination at 700°C. The resulting powders were annealed in air for 2 days at 1000°C and for two additional days at 1350°C to ensure homogeneity, and air-quenched.

The neutron diffraction data were collected with the five-detector powder diffractometer at the Research Reactor at the National Institute of Standards and Technology. The diffraction profiles were collected in steps of 0.05° 2θ for the range 15°–120° 2θ, with 1.5453-Å thermal neutrons monochromated by reflection from (220) of a Cu crystal.

ANALYSIS OF THE STRUCTURES

As the pyrochlore structure is a superstructure of a fluorite-like array of atoms, its diffraction pattern consists of a set of strong intensities representative of the average fluorite structure contained in a subcell plus an additional set of superstructure intensities. The structure factors for these intensities represent, respectively, the Fourier transform of the average scattering density in a subcell, and the Fourier transform of that function which, when added to the scattering density of the average structure, provides the distribution of density in the true superstructure. Buerger, in early definitive work (20), called the latter function the "complement structure." The superstructure intensities and their associated complement structure contain all of the information on the ordering process responsible for the formation of the superstructure. These intensities are, for the pyrochlore structure type, proportional to the difference in average scattering lengths of the *A* and *B* cation sites and thus to the extent of the ordering of species between the two sites for a particular composition. The superstructure intensities also depend on the scattering length of oxygen, the distribution of oxygen vacancies, and the displacement of O(1), in position 48f, *x* 1/8 1/8, from the ideal value $x = 3/8$ for an undistorted cubic array.

Neutron diffraction was a technique especially well suited to analysis of the present structures. The number of electrons associated with Y^{3+} and Zr^{4+} are identical ($Z_{Ti^{4+}} = 18$, $Z_{Y^{3+}} = 36$, $Z_{Zr^{4+}} = 36$, $Z_{O^{2-}} = 10$) causing these

species to be virtually indistinguishable in X ray diffraction in the absence of anomalous scattering. This, and the relatively small scattering power of oxygen, results in weak superstructure intensities. In contrast, the scattering lengths for thermal neutrons are $b_{Ti} = -0.3438$, $b_Y = 0.775$, $b_{Zr} = 0.716$, and $b_O = 0.581 \times 10^{-12}$ cm. The scattering length of oxygen is comparable to that of the cations, providing greater sensitivity to the distribution of oxygen vacancies and the distortion in the O(1) array. Moreover, the scattering length for titanium is *negative*. The difference between the scattering length of the individual cation sites and the small mean scattering length of a cation in the average substructure thus exceeds even the individual scattering lengths in the Ti-rich compositions. As a result, the superstructure intensities are larger than those of the substructure, Fig. 2, in marked contrast to the usual situation. This permitted reliable, systematic analysis of the solid solutions down to highly disordered states. The superstructure intensities did, nevertheless, decrease with increasing replacement of Ti by Zr, because

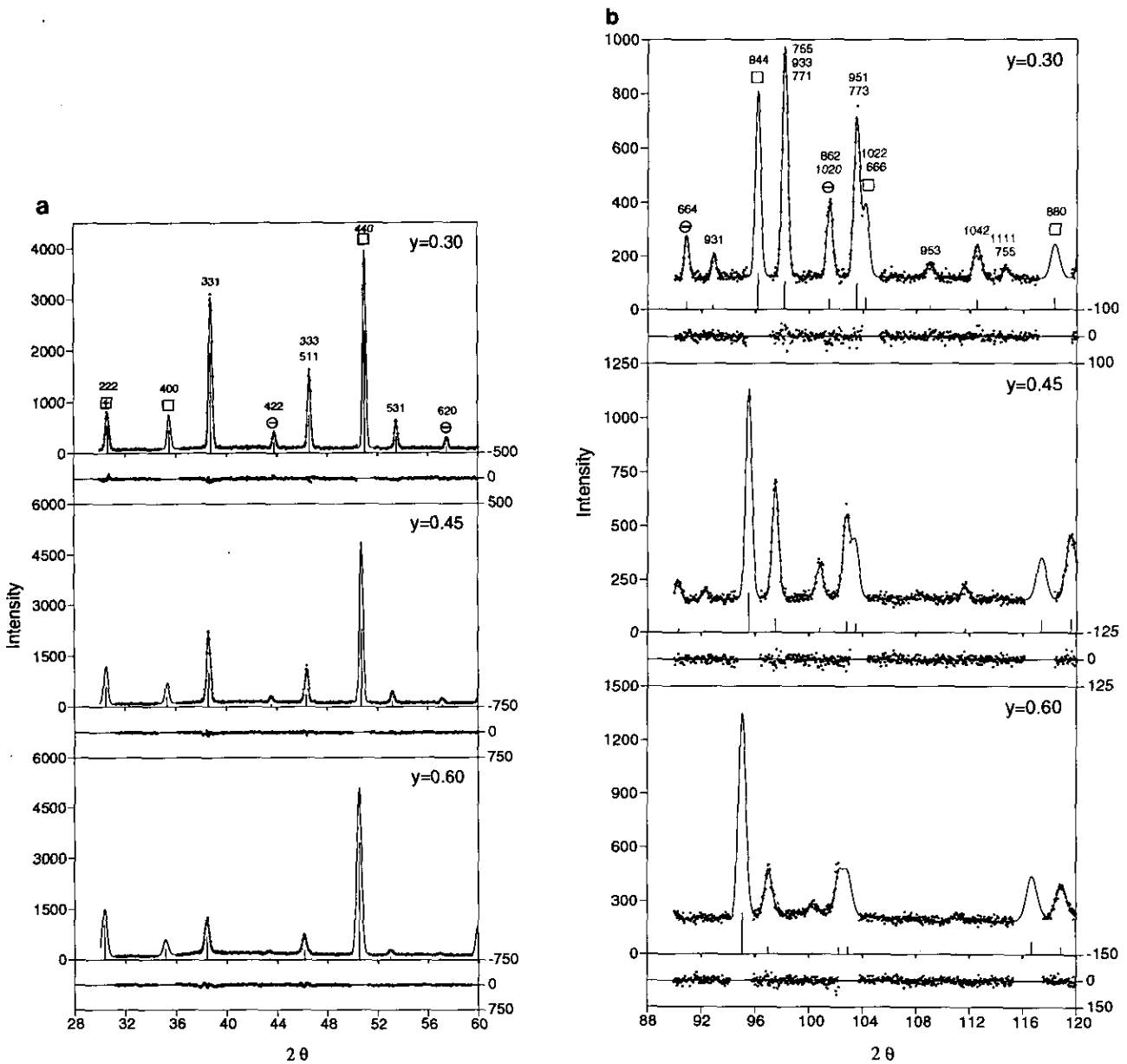

FIG. 2. Powder-diffraction patterns obtained with 1.5453-Å thermal neutrons for $Y_2(Zr_yTi_{1-y})_2O_7$ samples with $y = 0.30$, 0.45, and 0.60. (a) Low-angle diffraction profiles. (b) High-angle portion of the profiles. Experimental intensities are shown as data points; the continuous lines represent the fitted profiles. The difference between observed and calculated intensity, presented on the same scale as the profile, appears directly below each profile. Boxes indicate fluorite-like substructure intensities. A positive sign indicates an intensity maximum that receives only contributions from the cations and a negative sign those peaks to which only the anions contribute.

of both the similarity of the scattering lengths of Zr and Y and the increased extent of disorder induced by the substitution. The precision of the analysis thus declined with increasing y.

The present study was limited by the fact that a single diffraction experiment does not permit determination of the distribution of three species over two independent sites. The effective scattering lengths, b_A and b_B, of sites A and B are all that can be established, even in a refinement in which the occupancies are constrained to sum to the known bulk composition. As discussed elsewhere (21), refinement of a scattering length for, say, site A provides an experimental measure of

$$b_A = N_Y^A b_Y + N_{Zr}^A b_{Zr} + N_{Ti}^A b_{Ti}, \quad [1]$$

where N_i^A is the fractional occupancy of site A by species i. The scattering length of the B site is not independent due to the stoichiometric constraint

$$b_A + b_B = b_Y + y b_{Zr} + (1 - y) b_{Ti}. \quad [2]$$

Three additional relations follow provided both sites have unit occupancy:

$$N_Y^A + N_Y^B = 1 \quad [3]$$

$$N_{Zr}^A + N_{Zr}^B = y \quad [4]$$

$$N_{Ti}^A + N_{Ti}^B = 1 - y. \quad [5]$$

The above equations provide five relations in six unknown site occupancies. Additional information is necessary to specify the partitioning of cation species between the sites. We have, for one composition, recorded some initial diffraction patterns toward this end using synchrotron X radiation at wavelengths tuned to enhance anomalous scattering by the cation species. The results will be reported elsewhere.

No corresponding ambiguity exists for the determination of the anion distribution as only one scattering length is involved. The cell contents require

$$48 N_O^1 + 8 N_O^2 + 8 N_O^3 = 56, \quad [6]$$

where the fractional occupancies N_O^i refer to the 48f O(1), the 8a O(2), and the normally vacant 8b O(3) site, respectively. The occupancies may readily be determined in a constrained refinement of two independent and a third linearly dependent site occupancy.

The nature of the partially ordered pyrochlore superstructures created a subtle barrier to the analysis: the occupancy of no site in the structure is known a priori. The scale factor that relates observed and calculated intensities in the diffraction pattern therefore interacted strongly with the parameters (site occupancies, coordinates, and temperature factors) that define the superstructure. For example, if the calculated superstructure intensities were too small due to improper scaling, the distortion of the O(1) array and the difference in scattering length at the two cation sites both increased upon least-squares adjustment in order to provide larger superstructure intensities. This phenomenon led, in early stages of the refinement, to physically unreasonable values for the parameters, or to refinements that diverged. Fortunately, the fact that all ions occupy special positions in the space group permitted the minimization of correlation problems by the identification of classes of reflections that were independent of some features of the structural model. It was thus possible, by initial deletion of portions of the diffraction pattern, to separate the problem into a sequence of steps that permitted systematic independent determination of key features of the structure—most notably, the scale factor, distortion of the anion array, and the distribution of oxygen ion vacancies.

(1) Subcell reflections conform to the condition

$$hkl: \quad \begin{aligned} h + k &= 4n \\ k + l &= 4n \\ h + k &= 4n. \end{aligned} \quad [7]$$

Of these, a subset further obeying the condition

$$hkl: \quad \begin{aligned} h &= 4n + 2 \\ k &= 4n + 2 \\ l &= 4n + 2 \end{aligned} \quad [8]$$

receives no contribution from the anions and depends only on the sum of the cation scattering lengths in sites A and B. Deletion of all but these intensities from the profile permitted unambiguous refinement of the scale factor (plus the lattice constant and an average isotropic temperature factor for the cations) without knowledge of the cation distribution, the distribution of oxygen vacancies, or the distortion present in the O(1) array.

(2) Superstructure reflections that obey the set of conditions

$$hkl: \quad \begin{aligned} h &\neq 4n \\ k &\neq 4n \text{ with } h + k + l = 4n \\ l &\neq 4n \end{aligned} \quad [9]$$

receive contributions solely from the anion array. Refinements with all other intensities deleted from the pattern, and with the scale factor fixed at the value derived

in the first step, permitted a preliminary determination of the structural parameters for the oxygen ions (the coordinate x for O(1), temperature-factor coefficients, and occupancies of the three anion sites).

(3) All of the superlattice reflections were included in the refinement. As in the second step, all of the substructure reflections were excluded. Refinement of, first, the scattering lengths of the cation sites, and then the oxygen parameters as well, permitted the determination of all of the structural parameters of the pyrochlore structure. This step represents a refinement of the full complement structure.

(4) The subcell reflections were restored to the experimental profile and refinement was concluded with the complete data set. This step, which would normally have improved the agreement between observed and calculated intensity profiles for a superstructure, introduced unexpected complications, as discussed below.

REFINEMENT OF THE STRUCTURES

Profile refinement was performed with a version of Rietveld's refinement program (22), modified for the five-detector diffractometer by Prince. A total of 34 instrumental parameters were used to describe the profile: the zero-point in 2θ, six background parameters per detector, and three peak-shape parameters, U, V, and W used in an expression $H^2 = U \tan^2\theta + V \tan\theta + W$ to describe a Gaussian peak whose full width at half-maximum, H, increases with θ. The structural parameters were established through the sequence of steps described above. A total of 15 parameters were required: a scale factor, the lattice constant, the positional coordinate, x, for O(1), the scattering length of cation site A (that of site B was constrained by Eq. [2] as a dependent variable), two independent site occupancies for O(1) and O(2) (the occupancy of the interstitial site at 8b was treated according to Eq. [6] as a dependent variable). Isotropic temperature factors were assigned to all atoms in the early stages of the refinement. These were replaced by anisotropic temperature factors requiring a total of nine coefficients. Those for the anions were introduced in the final stages of step (2), those for the cations in step (3). A grand total of 49 parameters was thus employed in the description of the calculated diffraction profile.

We were unable to detect any superstructure intensities in the diffraction pattern of the sample with $y = 0.90$. Within the sensitivity of the analysis, therefore, the phase was treated as a defect-fluorite structure with no long-range order. The structure was, accordingly, refined in space group $Fm3m$ without the stepwise analysis outlined above. The high symmetry at the sites occupied in the fluorite array precludes anisotropy in the thermal motion. Three structural parameters—a lattice constant and two temperature-factor coefficients—sufficed for description of the structure.

Refined parameters for all of the compositions that were examined are presented in Table 1. The following discussion of the change in structure with composition also includes parameters obtained in an analysis of $Y_2Ti_2O_7$ ($y = 0$) by Haile *et al.* (21).

EVIDENCE FOR A COEXISTING FLUORITE-LIKE PHASE

The entire powder diffraction profile was employed in the refinement in the final stage of analysis described above. Inclusion of the superstructure maxima in the profile would normally result in further reduction of the residuals as these peaks are intense, have low standard deviations, and depend only upon the average structure. The opposite occurred, as can be seen from the residuals summarized in Table 2. The structural parameters of Table 1 were used in these refinements. The scale factor was also held constant. Only the lattice constant and peak-shape parameters were adjusted.

It may be seen that the lattice constant has increased by a small but statistically significant amount. The peak-shape parameters have also changed as the substructure intensities were typically narrower than the superstructure peaks at low θ, but broadened more rapidly at higher angles. The difference between the observed and calculated diffraction profiles revealed significant residual intensity at the location of the substructure peaks for which the pyrochlore structure alone was unable to account. This was the major source of the increase in the residuals.

The parameters of Table 1 were determined through a valid refinement of the complement structure and thus represent a description of the pyrochlore phase that constitutes the predominant volume fraction of the specimens. We intepret the shift in lattice constant and the unaccounted intensity in the substructure peaks as indication of the coexistence of a second fluorite-like phase with a lattice constant slightly larger than $a/2$ of the pyrochlore superstructure and that was present in an amount that increased with y. A similar increase in lattice constant has been frequently observed upon disorder in alloys such as CuZn or phases in the Cu–Au system that also undergo order–disorder transformations (23). The increased lattice constant of the second phase might also have arisen from a slightly higher content of the larger Zr ion. However, the anomaly cannot be interpreted as a miscibility gap between a pyrochlore phase and a fluorite-like phase of different composition. In this case one would have two phases of fixed lattice constants in relative amounts that changed with y. Instead, the lattice constant of the fluorite phase always remained very close to half that of the pyrochlore component. Attempts were made to determine the presence and size of any fluorite-type domains with the

TABLE 1

Values of the Lattice Constant, Atomic Coordinates, Site Occupancies and Anisotropic Temperature-Factor Coefficients for $Y_2(Zr_yTi_{1-y})_2O_7$ Based on Refinements of the Complement Structure—That Is, Refinement with Portions of the Powder Diffraction Profile That Consisted Only of the Superstructure Reflections

Site	Superstructure			Fluorite
	y 0.3	0.45	0.6	0.9
a (Å)	10.1901(2)	10.2437(3)	10.2810(5)	10.3858(1)
A in 16 c $\bar{3}m$ 0 0 0				
b/b_Y	1.00(5)	1.00(3)	0.992(3)	0.895
$\beta_{11} = \beta_{22} = \beta_{33}$[a]	0.0009(1)	0.0026(3)	0.0046(6)	0.0046(1)
$\beta_{12} = \beta_{13} = \beta_{23}$	−0.0005(1)	−0.0005(1)	−0.0001(2)	0
B in 16d $\bar{3}m$ 1/2 1/2 1/2				
$\beta_{11} = \beta_{22} = \beta_{33}$	0.0009(1)	0.0052(23)	0.0062(15)	0.0046(1)
$\beta_{12} = \beta_{13} = \beta_{23}$	−0.0005(1)	0.0024(11)	−0.0026(6)	0
O(1) in 48f mm x 1/8 1/8				
N	0.994(1)	0.957(1)	0.922(3)	0.875
x	0.4173(2)	0.4110(2)	0.4022(3)	0.375
β_{11}	0.0041(1)	0.0075(1)	0.0087(3)	0.0096(1)
$\beta_{22} = \beta_{33}$	0.0030(1)	0.0036(1)	0.0049(2)	0.0096(1)
β_{23}	−0.0004(2)	−0.0003(2)	0.0008(4)	0
O(2) in 8a $\bar{4}3m$ 1/8 1/8 1/8				
N	1.00(5)	1.00(3)	0.97(2)	0.875
$\beta_{11} = \beta_{22} = \beta_{33}$	0.0018(1)	0.0017(2)	0.0026(4)	0.0096(1)
O(3) in 8b $\bar{4}3m$ 3/8 3/8 3/8				
N	0.036	0.258	0.488	0.875
$\beta_{11} = \beta_{22} = \beta_{33}$	0.005(3)	0.010(2)	0.012(3)	0.0096(1)
U	3993(21)	4751(210)	4727(502)	3761(66)
V	462(30)	1036(56)	1756(161)	243(22)
W	815(10)	1183(18)	2120(49)	695(5)
R_B (%)[b]	4.10	3.72	8.21	2.95
R_P (%)[c]	6.42	6.22	6.50	6.02
R_{WP} (%)[d]	8.67	8.10	8.27	8.06
R_E (%)[e]	7.87	7.51	7.13	7.21

Note. Standard deviations are in parentheses.

[a] The temperature factor is defined as $\exp -(h^2\beta_{11} + k^2\beta_{22} + l^2\beta_{33} + 2hk\beta_{12} + 2kl\beta_{23} + 2hl\beta_{13})$.

[b] $R_B = (\Sigma\,|I_B(\text{obs}) - (1/c)I_B(\text{cal})|)/\Sigma\, I_B(\text{obs})$, where I_B is the integrated intensity of the individual Bragg peak and c is the scale factor.

[c] $R_P = (\Sigma\,|Y_i(\text{obs}) - (1/c)Y_i(\text{cal})|)/\Sigma\, Y_i(\text{obs})$, where Y_i is the intensity at $2\theta_i$.

[d] $R_{WP} = \{[\Sigma\, w_i(Y_i(\text{obs}) - (1/c)Y_i(\text{cal}))^2]/\Sigma\, w_iY_i^2(\text{obs})\}^{1/2}$, where w_i is the weight assigned to Y_i in proportion to the reciprocal of the square of its standard deviation.

[e] $R_E = \{(n-p)/\Sigma\, w_iY_i^2(\text{obs})\}^{1/2}$, where n is the number of observations and p is the number of variable parameters employed in the least-squares refinement.

aid of high-resolution transmission electron microscopy and with dark-field microscopy. Unfortunately, as the oxygen ions are very mobile, the specimens disordered very rapidly in the electron beam.

The presence of a fluorite-like component has, however, been confirmed in high-resolution powder-diffraction patterns obtained with synchrotron X radiation for the sample with $y = 0.60$. The profiles of the substructure intensities in this pattern displayed asymmetry that strongly suggested the presence of a shoulder at lower θ. The profiles could indeed be more satisfactorily fit with two, rather than one, pseudo-Voigt functions, by amounts that were statistically significant. The integrated intensities of the fluorite-like peaks proved to be 10–12% of the total intensity in a substructure peak. The major component of the doublet yielded a lattice constant very close to the refined value for pyrochlore that was obtained through neutron Rietveld analysis of the complement structure. The minor fluorite component had a lattice constant 0.0062 Å larger than $1/2a$ for pyrochlore. It should be

TABLE 2

Lattice Constants, Peak-Shape Parameters, and *R* Factors for Refinements Based on the Total Pattern, But Using the Structural Model Obtained in Table 1

y	0.3	0.45	0.6
a (Å)	10.1906(2)	10.2447(2)	10.2890(5)
U	4461(113)	5634(149)	6661(241)
V	528(66)	1151(47)	2003(80)
W	781(57)	972(11)	1246(17)
R_B(%)	7.57	6.04	7.40
R_P(%)	7.56	7.26	8.44
R_{WP}(%)	10.21	9.61	11.24
R_E(%)	7.37	6.85	6.27

noted in passing that, strictly speaking, the presence of a contribution from the fluorite phase to the pyrochlore substructure intensities negates the validity of the first step of the refinement process in which the scale factor was established. Fortunately, the fact that the contribution was less than 12% of the total substructure intensity in any sample allowed a determination of scale factor that was sufficiently precise to allow the refinement process to proceed successfully to convergence.

RESULTS AND DISCUSSION

The measured intensities in the powder diffraction profiles are shown as discrete data points in representative patterns presented in Fig. 2. These fits between calculated and observed intensity provided the structural parameters of Table 1. The subcell reflections have therefore been excluded. The calculated profiles are shown as continuous lines fitted to the data points. Also shown, below each profile, are the differences between the observed and calculated intensities plotted to the same scale. The patterns, especially for small and intermediate y, may be seen to consist of sharp, clearly separated peaks, well described by a Gaussian peak-shape function. Measurable peak intensity and resolved maxima persist in the pattern to 120° 2θ, the limit to which data were recorded. Consequences of the increased amount of disorder that accompanies increases in y may be noted in the patterns: decreases in the relative magnitude of the superstructure intensities, undulations in the background intensity, and broader superstructure maxima with growing indication of non-Gaussian "tails." The background features are especially apparent in the patterns for $y = 0.90$ (see Fig. 3).

Variation of Structural Parameters with Composition

A plot of the lattice parameter as a function of increasing content, y, of the larger Zr^{4+} ion, Fig. 4, shows very linear behavior in accord with Vegard's law. A fit to the pyrochlore lattice constants for $y = 0$ through 0.60 provides

$$a\ (\text{Å}) = 10.0959 + 0.3154y. \qquad [10]$$

Individual data conform to the relation to, on average, within 0.003 Å or about 10σ. Part of the scatter undoubt-

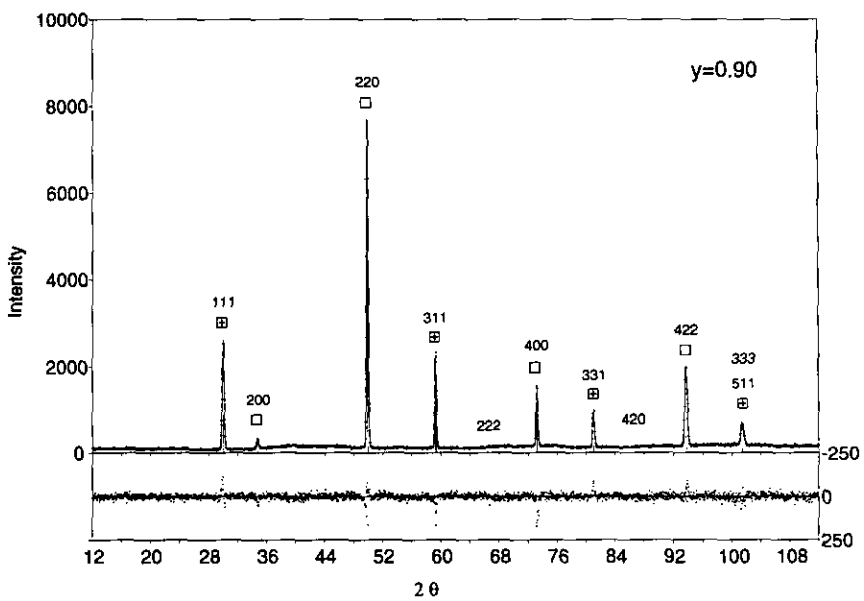

FIG. 3. A portion of the powder diffraction pattern obtained with 1.5453-Å thermal neutrons for $Y_2(Zr_{0.9}Ti_{0.1})_2O_7$, fully disordered to the defect fluorite structure type. The measured intensities are indicated by discrete data points, the fitted profile with continuous lines. The differences between the measured and calculated intensities are plotted beneath the profile on a scale expanded by a factor of four. The intensities have been indexed relative to the fluorite cell.

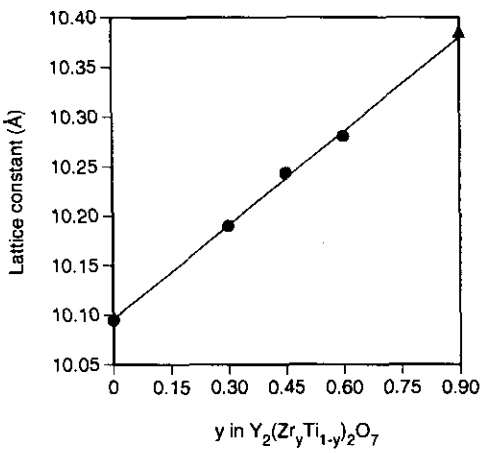

FIG. 4. Variation of the pyrochlore lattice constant as a function of Zr^{4+} content, y. The value plotted for the solid solution with $y = 0.90$, which has a disordered fluorite structure, is twice the lattice constant of the defect fluorite cell. This datum was excluded from the linear relation fit to the lattice constants of the pyrochlore-type phases.

edly arises from small differences between the actual and nominal composition of the samples. Twice the lattice constant of the fluorite cell for the sample with $y = 0.90$ is also included in Fig. 4. The result falls above the fit to the lattice constants of the pyrochlore phases by 0.0060 Å. As noted above, the lattice constant of the pyrochlore phase with $y = 0.60$ was also smaller than twice that of the disordered fluorite phase with which it coexisted.

Figure 5 shows the effect of Zr substitution on the positional parameter, x, for O(1). The amount of displacement toward the vacant anion position at 8b decreases from 0.4625 Å to zero as x decreases from 0.42082 for $y = 0$ (21) to 0.375 for the ideal cubic array of anions in the fully disordered fluorite state. The variation of the O(1) coordinate with y for $0 \leq y \leq 0.6$ very closely obeys the quadratic relation

$$x = -0.06364y^2 + 0.007085y + 0.42081. \quad [11]$$

Individual refined coordinates deviate from this relation by, on average, only $(1/3)\sigma$. As samples were prepared at discrete intervals in y, the present analyses have established only that the Zr content at which long-range order has disappeared falls somewhere in the range $0.60 < y \leq 0.90$. The close fit of the experimental O(1) coordinates to Eq. [11], and the rapid decrease in x as the disordered stated is approached, suggests that extrapolation of Eq. [11] beyond $y = 0.60$ to the ideal coordinate 3/8 might provide an estimate of the composition that marks the onset of complete disorder. Equation [11] predicts that x would be 0.3756 for a composition with $y = 0.9$, a value that differs from 3/8 by only 2 to 3 standard deviations for the experimentallty determined coordinates. Conversely, Eq. [11] predicts $x = 3/8$ at a composition $y = 0.906$. Given limits on the sensitivity with which complete absence of any superstructure maxima may be detected, as well as lack of knowledge of the extent to which true values of y deviate from the nominal compositions, it appears that our sample with $y = 0.90$ fortuitously marks the effective onset of complete structural disorder.

Table 1 shows that the anisotropic temperature-factor coefficients for all atoms tend to increase with increasing y, indicative of a general softening of the structure with increasing disorder. The thermal parameters of O(1), shown in Fig. 6, show a progressive increase of anisotropy with increasing y until complete disorder to the fluorite structure requires isotropic thermal displacement. The fact that $B_{11} > B_{22}$ indicates an increased thermal vibration amplitude (and thus a shallower potential barrier) toward the initially vacant 8b site as well as an overall softening of the potential with increasing y.

Change in Disorder in the Cation and Anion Arrays with Zr Content

Figure 7 presents the variation of site occupancies in the anion array as a function of Zr content, y. The first symptom of disorder in the pyrochlore structure arises with partial filling of the ideally empty site at 8b with oxygen ions that originate solely from the 48f O(1) site. The result is not surprising as the O(1) sites form the nearest-neighbor oxygen shell of the vacant 8b site. The O(2) sites may be seen to participate in the disordering process only at higher Zr concentrations. Complete disorder results at $y = 0.90$ when the occupancy of all anion

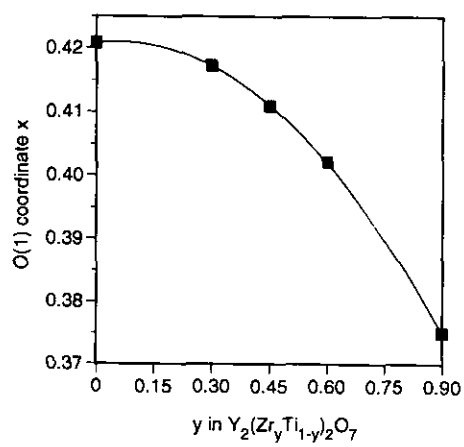

FIG. 5. Relaxation with increasing Zr^{4+} content, y, of the O(1) coordinate $x = \frac{3}{8} + \Delta$ (where Δ is the displacement in the direction of the unoccupied or partially occupied O(3) site) toward the ideal position of an undistorted cubic array of anions. The variation closely follows a quadratic relation. The result for the defect-fluorite solid solution found when $y = 0.90$ has not been included in the fitted function. The relation extrapolates to a coordinate of $\frac{3}{8}$ at $y \approx 0.90$ suggesting that this composition marks the onset of loss of long-range order.

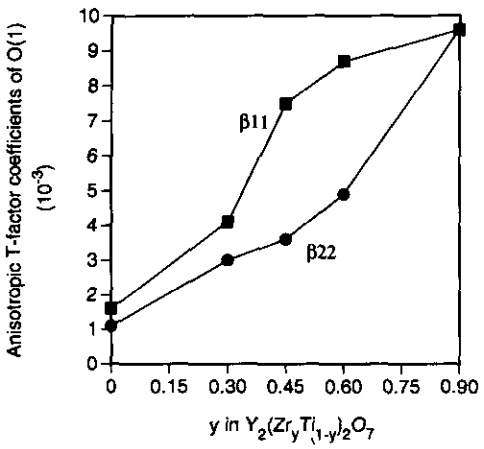

FIG. 6. Variation of β_{11} and $\beta_{22} = \beta_{33}$, the anisotropic temperature-factor coefficients for O(1), as a function of the Zr^{4+} content of the solid solutions. As $\beta_{11} > \beta_{22}$ the thermal vibration amplitude is largest along x in the direction of the partially occupied O(3) site. The increase of both coefficients with y indicates a general softening of the structure with increasing Zr^{4+} content.

sites is 0.875. The partial occupancy of O(2) never decreases to a value equal to the occupancy of O(1) at any composition with y less than that of the fully disordered defect fluorite state.

The progress of disorder in the anion array may also be described in terms of change in a set of order parameters, S, defined such that their value changes from unity for complete order to zero for the defect fluorite state when all site occupancies are 7/8. Appropriate definitions are

$$S_{O(1)} = [N_O^1 - 7/8]/(1 - 7/8) \quad [12]$$

$$S_{O(2)} = [N_O^2 - 7/8]/(1 - 7/8) \quad [13]$$

and

$$S_{O(3)} = [(1 - N_O^3 - 1/8]/(1 - 1/8). \quad [14]$$

As the occupancy of the normally vacant O(3) site at 8b is a constrained, linearly dependent parameter, Eq. [6], the order parameter $S_{O(3)}$ is a weighted average of the order parameters of the two other sites:

$$S_{O(3)} = (6/7)S_{O(1)} + (1/7)S_{O(2)}. \quad [15]$$

The variation of these anion order parameters with y, Fig. 8, clearly shows the different rates at which the three sites disorder.

Our experimental measure of the extent of disorder in the cation array is the refined scattering length for site A. As noted above, this scattering length can arise from an appreciable range of partitionings of the three cation species for a particular composition and, moreover, the total scattering density distributed over the A and B sites increases with y. We therefore report the result in Table 1 as b_A/b_Y, the experimental scattering length relative to that of yttrium. The measured variation of b_A/b_Y with y is shown in Fig. 9. The predictions of several limiting models of the disorder are included for comparison. The ratio would remain unity for all compositions if Zr merely replaced Ti on the B site. If all of the Zr ions are placed in the A site, leaving Ti on the B site along with the displaced Y ions, the variation of b_A is

$$b_A/b_Y = [b_Y + y(b_{Zr} - b_Y)]/b_Y. \quad [16]$$

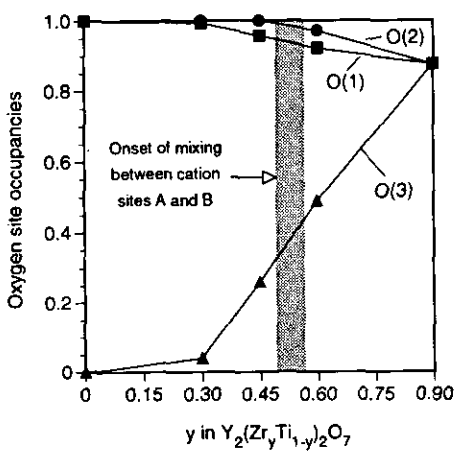

FIG. 7. Change in the occupancy of the anion sites as a function of increasing Zr^{4+} content of the pyrochlore solid solutions. Underoccupancy of the 48f O(1) site—the nearest-neighbor anion shell about the normally vacant O(3) site—begins at low Zr^{4+} content. Disorder involves the O(2) site only halfway through the solid solution series after the onset of mixing of the occupancies of the cation sites.

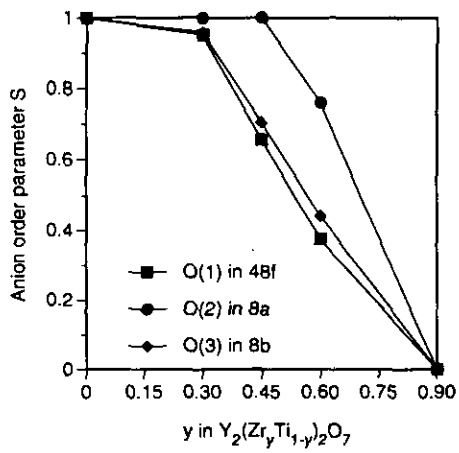

FIG. 8. Variation of the order parameters of the three independent anion sites as a function of Zr^{4+} content, y. Disorder among the three sites clearly progresses at different rates.

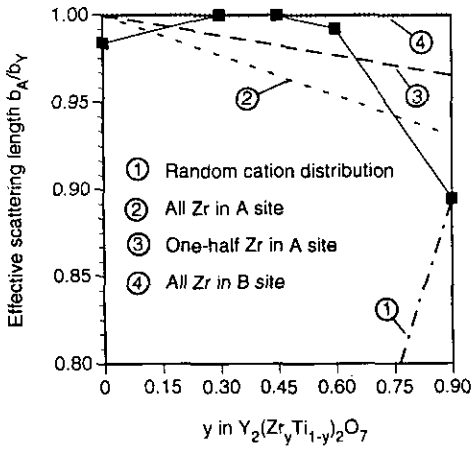

FIG. 9. The effective scattering length at cation site A relative to the scattering length of Y^{3+} as a function of changing Zr^{4+} content, y, of the solid solutions $Y_2(Zr_yTi_{1-y})_2O_7$. Curves (1) through (4) present the predicted variation for several assumed distributions of the substituted Zr^{4+} ions. The fact that $b_Y > b_{Zr} \gg b_{Ti}$ and $b_A \approx b_Y$ for most of the range of solid solution means that Zr^{4+} replaces only Ti^{4+} in the B sites. Mixing of the contents of A and B cation sites occurs only at compositions close to the onset of complete disorder.

If the substituted Zr ions are placed with equal probability in the A and B sites,

$$b_A/b_Y = [2b_Y + y(b_{Zr} - b_Y)]/2b_Y. \qquad [17]$$

For a completely random distribution of cations, b_A and b_B are equal and given by one-half the scattering length provided by the constraint of stoichiometry, Eq. [2].

The variation of b_A with y displayed in Fig. 9 shows that b/b_Y is unity for $y \leq 0.45$. As $b_{Zr} < b_Y$ and b_{Ti} is negative, this requires that the A site be entirely occupied by Y for about one-half of the solid solution series; the substituted Zr replaces only Ti ions in the B site. It is worth noting that, at $y = 0.45$, there is significant underoccupancy of the O(1) site and that the interstitial site is more than one-quarter filled! The O(2) site, which forms the nearest-neighbor shell for cation site A, is still fully occupied. The disorder in the cation array and the oxygen sites therefore proceed independently. Only at $y = 0.6$ does mixing between the cations occur and this is accompanied by the onset of vacant sites among the O(2) that surround cation site A.

It is curious that $Y_2Ti_2O_7$, $y = 0$, was found (21) to have a completely ordered oxygen ion array, yet a small (but statistically significant) replacement of Y^{3+} by Ti^{4+}. The occupancy of site A that corresponds to the value of b_A listed in Table I is $Y_{0.988(4)}\,Ti_{0.012}$. It is not clear why such disorder should be found only for pure yttrium titanate.

At $y = 0.60$ measurable mixing of cations has occurred between sites A and B. We are as yet unable to specify whether it is Zr^{4+} or Ti^{4+} (or both) that have entered site A. However, b_A falls considerably above the scattering length predicted, Fig. 9, if half of the substituted Zr^{4+} had entered site A. Limits may be placed on the amounts of either Zr^{4+} or Ti^{4+} responsible for the decrease in b_A if one assumes that only one species or the other has entered the site: 0.1314(4) Zr^{4+} or 0.007(3) Ti^{4+}. The majority of the Zr^{4+} at $y = 0.60$ has thus continued to enter site B to replace Ti^{4+}. For $0.60 < y < 0.90$, however, there is rapid onset of complete mixing of all cation species as the defect fluorite structure is assumed.

Fourier Synthesis of Scattering Density and Comparisons with Theoretical Predictions

The structural changes that are described above are clearly apparent in Fourier syntheses of the scattering density within the cell.[1] Figure 10a presents the scattering density $\rho(x\ y\ 0)$ for the compositions with $y = 0.30$, 0.45, and 0.60. This section passes through cation sites A and B. It is interesting to follow the replacement of a weak "negative atom" at site B ($b_B = -0.0259 \times 10^{-12}$ cm for $y = 0.30$) by positive density as y is increased. Figure 10b provides the scattering-density sections $\rho(x\ y\ 1/8)$. These sections display the scattering density at all three oxygen ion locations (but pass through the centers of only 4/6 of the O(1) ions). The displacement of O(1) from the ideal location $x = 3/8$ of an undistorted cubic array of ions is apparent both in the displacement toward the vacant site for the O(1) that are located in the plane of the section and in the diminished weight of the peaks for the two O(1) ions that do not lie at $z = 1/8$. The progressive relaxation of this distortion with increasing y may be followed in the maps.

Modeling of the disorder and calculation of the energies for defect formation in the pyrochlore structure have been undertaken by several workers. Preliminary results (24) for Gd and Y titanate and zirconate suggest that displacement of O(1) from position 48f to the unoccupied site at 8b requires an energy of ca. 5 eV, sufficiently large that the vacancies at the O(3) location are effectively "locked into" their positions for a pyrochlore in which the cations are fully ordered. Disorder in the cation array reduced the calculated energy by a factor greater than two. Our results differ from that prediction in so far as displacement of O(1) into the 8b interstice begins well before any mixing

[1] The coefficients used in the summations were F_{obs} in the case of the superstructure reflections. Values of F_{cal} were used instead of F_{obs} for the substructure reflections as the measured intensities contained a contribution from the coexisting fluorite phase. The substructure reflections depend only on the average structure and are insensitive to the details of the structural model. No significant departure from a normal representation of the scattering density is likely. The contribution of the average structure will vanish in the difference maps of Fig. 11 as a consequence of this approximation. The maps of $\rho_{obs} - \rho_{cal}$ are thus, rigorously, difference maps for the complement structure.

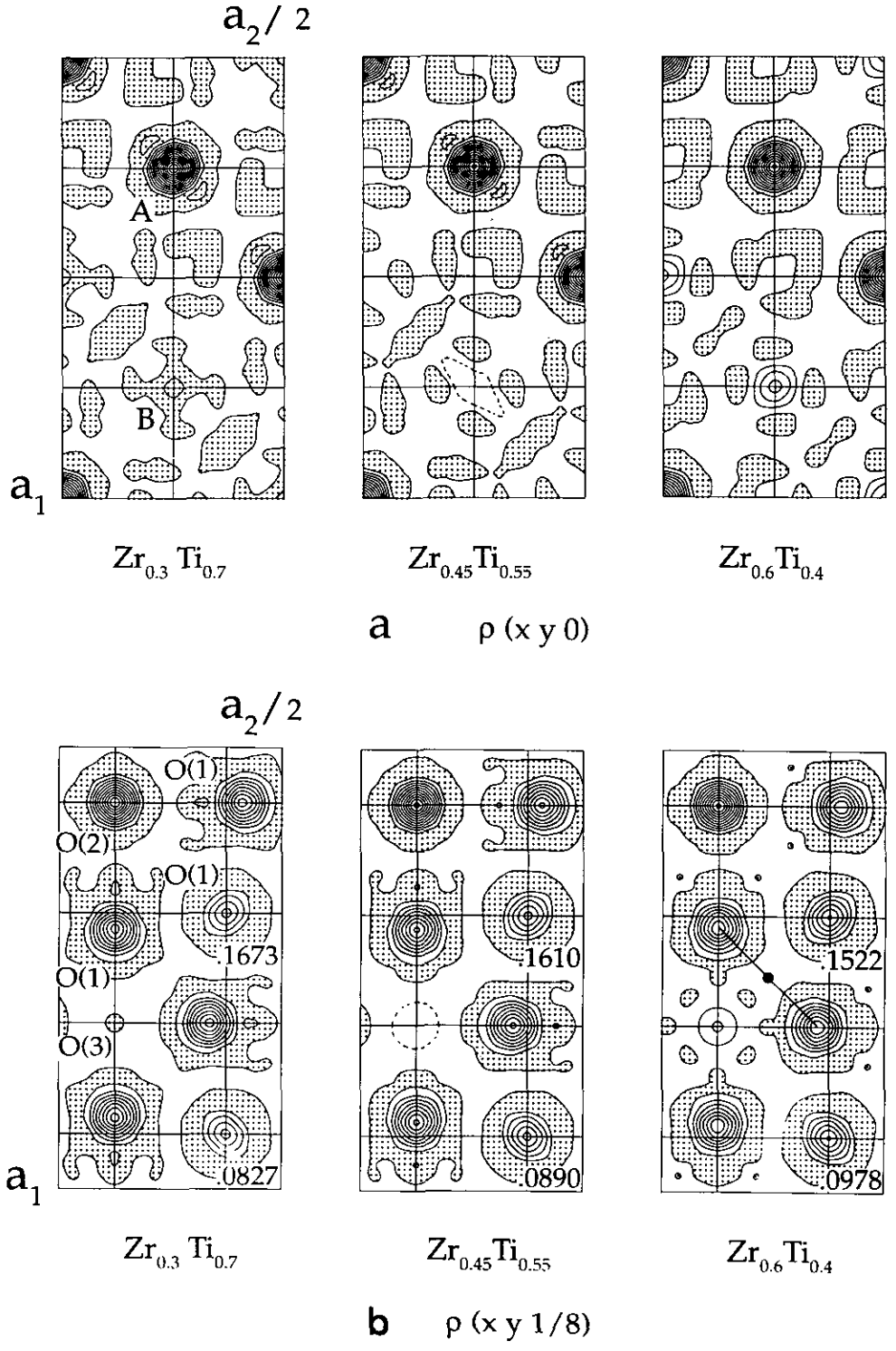

FIG. 10. Fourier syntheses of the scattering density in $Y_2(Zr_yTi_{1-y})_2O_7$ pyrochlores. Contour intervals at 200×10^{-12} cm $\times a^3$, where a is the lattice constant (i.e., the summation has not been scaled by the reciprocal of the cell volume). Regions of negative density are shaded. The dashed contours at cation site B and at the position of O(3) for $y = 0.45$ are at half the interval employed elsewhere. They are included to show that the scattering density is not flat, but rather that a small but well-defined positive peak is present at these sites. (a) Sections $\rho(x\ y\ 0)$ for solid solutions with $y = 0.30$, 0.45, and 0.60. These sections pass through cation sites A and B. The progressive change of B from a "negative atom" to a site with positive scattering length may be noted. (b) Sections $\rho(x\ y\ \frac{1}{8})$ for $y = 0.30$, 0.45, and 0.60. These sections pass through O(2), the normally vacant O(3) site and four of the six O(1) sites that appear. The z coordinate of the O(1) ions displaced from the plane of the section is noted. The displacement of O(1) toward the vacant O(3) site may be observed along with the relaxation of this distortion with increasing y. The section for $y = 0.60$ shows, by means of a small filled circle, the location of an interstitial site between a pair of O(1). Proposed as part of a vacancy-interstitial complex by van Dijk *et al.* (25), the present maps are not able to provide evidence for occupancy of this site. Progressively increased occupancy of the O(3) site at 8b is, however, confirmed.

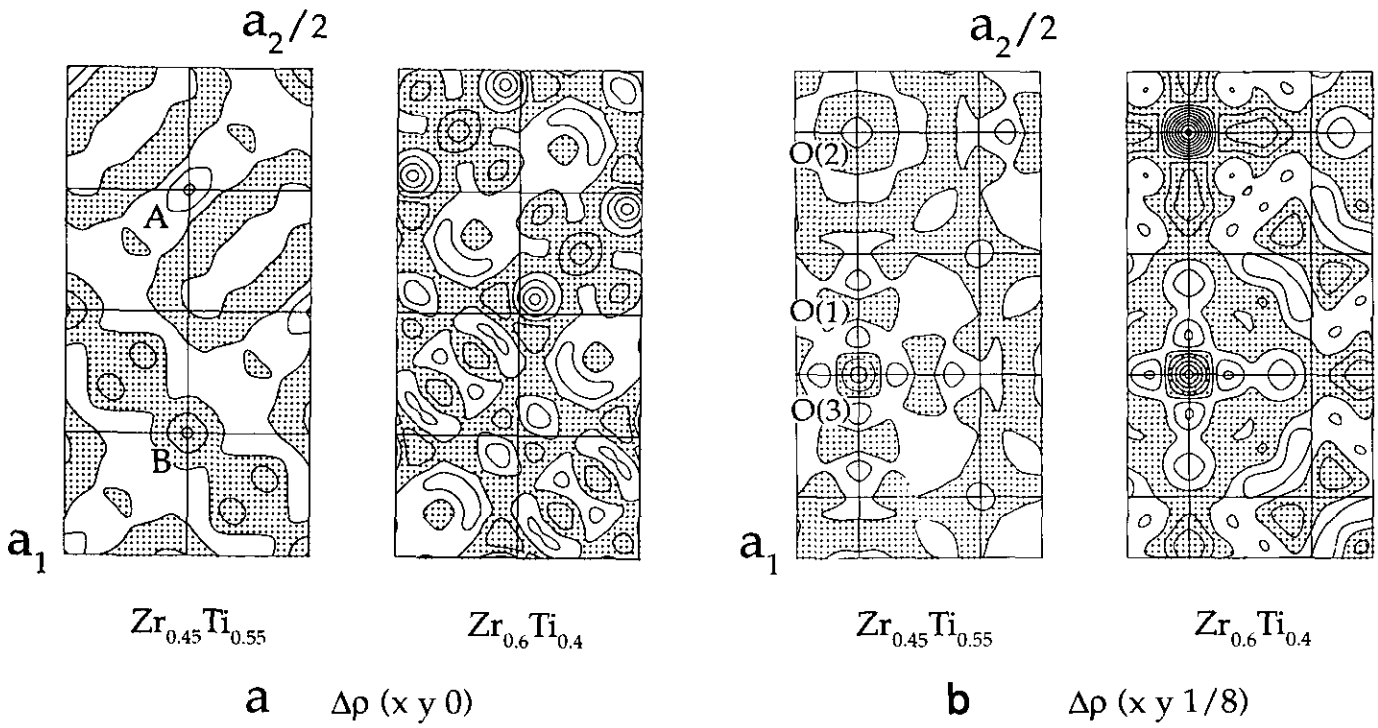

FIG. 11. Fourier synthesis of the difference density $\rho_{obs} - \rho_{cal}$ for $Y_2(Zr_yTi_{1-y})_2O_7$ pyrochlores. Contour intervals at 10×10^{-12} cm $\times a^3$, a scale expanded 20-fold relative to the contour interval of Fig. 10. Regions of negative density are shaded. (a) Sections $\Delta\rho(x\ y\ 0)$ for solid solutions with $y = 0.45$ and 0.60. No significant anomalies occur at cation sites *A* or *B*. (b) Sections $\Delta\rho(x, y, \frac{1}{8})$ for $y = 0.45$ and 0.60. Anomalies at the sites of O(2) and O(3) suggest that too much scattering density in the model structure has been assigned to the interstitial position at the expense of O(2), but the difference corresponds to about 0.03 oxygen atom, on the order of the standard deviation in the refined site occupancy.

between the occupancies of the cation sites at 16c and 16d has occurred. Replacement of Ti^{4+} in site *B* by some Zr^{4+} is necessary, however, to promote the displacement of O(2). The energies calculated for this process, it must be noted, seem to be for pyrochlores that are binary in terms of their cation content so that disorder between the occupancies of sites *A* and *B* would be the only type of cation mixing that is possible. Involvement of O(2) in the disorder does indeed appear to be coupled to mixing between the cation sites in our results.

Van Dijk *et al.* (25) computed that in $Gd_2Zr_2O_7$ the most stable oxygen Frenkel defect should involve an O(1) vacancy and O(3) interstitial, requiring 1.96 eV per defect. They also proposed that a linear complex, consisting of a pair of O(1) vacancies with an interstitial anion midway between, might be more stable (by 0.2 eV) than a simple oxygen vacancy. The location of the interstitial anion was not specifically stated, but a figure that depicted the environment of the complex showed that it lies along $[0\bar{1}1]$ and appears to be parallel to (100). The interstitial therefore would occupy the site indicated by a small filled circle shown in the scattering density map $\rho(x\ y\ 1/8)$ for $y = 0.60$ in Fig. 10b. This site corresponds to position 96g *xxz* in space group $Fd3m$, with $z = 3/8$. The *x* coordinate of the position must be a function of the *x* coordinate for O(1), if the interstitial is to be midway between a pair of these ions. It may be shown that $x = 1/4 + \Delta/2$, where $\Delta = x_{O(1)} - 3/8$ is the distortion of O(1) from the ideal site of a regular cubic array of anions.

The scattering density maps of Fig. 10b provide no evidence for occupancy of this site, nor do the corresponding difference density maps, Fig. 11b. Instead, Fig. 10b shows progressively increasing density in the O(3) site as a consequence of disorder in the arrangement of anions. It may be noted, however, that only a region of weak negative density appears at the O(3) site in $\rho(x\ y\ 1/8)$ for the solid solution with $y = 0.30$. This is due to background fluctuations in these maps due to the "Fourier ripple" that arises from series termination error in the summations. We estimate these fluctuations to be on the order of ca. 70×10^{-12} cm $\times a^3$ or 6.6×10^{-10} cm/Å^3. This is about one-third of the contour interval employed in Fig. 10. The magnitude of these fluctuations relative to the scattering density at the fully occupied anion sites suggests that a minimum anion site occupancy on the order of 0.035 may be discerned in the maps. This is about the same magnitude as the refined occupancy for the O(3) site, 0.040, at composition $y = 0.30$. For similar reasons, the very large number of sites per cell for the 96g interstitial in the split-vacancy complex precludes the extraction

of information on the occupancy of this site from the maps: If the 7/8 anion of the fully disordered structure was distributed over this position rather than placed at O(3), the occupancy of each available 96g site would amount to 0.0091, far below the limit of detectability.

Although the present results cannot totally exclude the presence of the 96g interstitial/split-vacancy complex—perhaps as a minority defect—the scattering density maps provide clear evidence for occupancy of the O(3) site. The maxima in the scattering density at the O(3) site are in the ratio 0.43 for the samples with $y = 0.45$ and 0.60 (the temperature factors for O(3) are essentially equal at these two compositions) compared to a ratio for the refined occupancies of the site of 0.53. An approximate numerical integration of the scattering density associated with each anion peak provides site occupancies at $y = 0.45$ that are in the ratio 0.98 : 1.0 : 0.2 for O(1), O(2), and O(3) respectively. The refined site occupancies are 0.957(1), 1.00(3), and 0.26. Occupancy of the O(3) site in Fourier syntheses and difference maps was also observed when this ion was omitted from the structural model to avoid biasing the resulting maps. There is, therefore, no compelling evidence for "missing" anion scattering density and we conclude that O(3) is the site of the primary defect in the anion array.

The primary mechanism for the high levels of oxygen ion conduction in $Y_2(Zr_yTi_{1-y})_2O_7$ pyrochlores is likely a jump between nearest-neighbor O(1) sites as the arrangement of these ions provides a continuous path for migration through the structure. This view is supported by modeling (25). However, the migration energy is on the order of 0.9 eV. When used in a Boltzmann factor, this predicts far too small a scattering density at the saddle point of the jump to permit detection in a Fourier map. We are thus unable to provide insight into whether the jump proceeds directly along ⟨100⟩ between adjacent O(1) sites (25), or follows a path that moves through the octahedral interstice in the cation array (14). Jumps between 48f sites are possible only if vacancies exist in the O(1) array. These are created by displacement of O(1) to the vacant 8b sites. The ionic electrical conductivity measured for $Y_2(Zr_yTi_{1-y})_2O_7$ pyrochlores by Moon (15, 16) is shown in Fig. 12 as a function of Zr^{4+} content and temperature. The conductivity isotherms are approximately parallel, indicating that the activation energy is not strongly dependent upon composition. Besides the possible dependence on other material parameters that may vary with composition, the magnitude of the conductivity should be proportional to the product of charge-carrier density and the number of vacant sites to which the charge carriers may jump—that is, $N(1 - N)$ where we here take N to be the site occupancy of O(1) measured in the present work. The variation of this product with y, included in Fig. 12, provides a satisfactory qualitative explanation for both the magnitude of the change in ionic conductivity and its dependence on composition, except for the behavior in highly ordered phases at small y. The conduction properties of the latter solid solutions are likely to depend on the influence of accidental impurities. A more quantitative use of the structural data in the interpretation of fast-ion conduction in these materials will be the subject of future work.

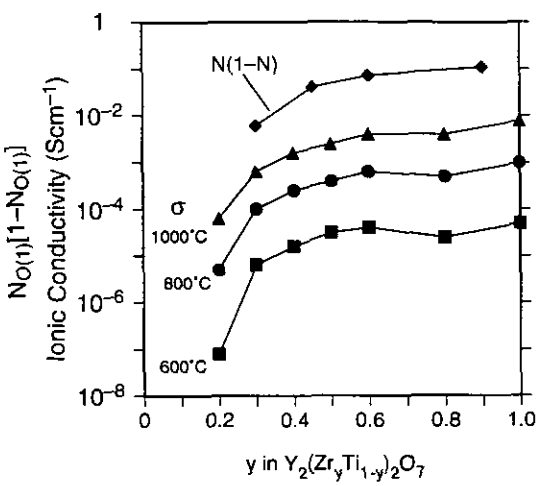

FIG. 12. Ionic electrical conductivity for $Y_2(Zr_yTi_{1-y})_2O_7$ solid solutions as a function of temperature and Zr^{4+} content, y. Included in the plot is the variation of the product of charge-carrier concentration and vacancy concentration $N(1 - N)$, where N is taken as the site occupancy of the O(1) site at 48f. The change of this product with y provides a satisfactory qualitative explanation of both the magnitude of the conductivity change and its dependance on composition.

CONCLUSIONS

The present structural study of four phases ($y = 0.30$, 0.45, 0.60, and 0.90) in the $Y_2(Zr_yTi_{1-y})_2O_7$ system has shown that their structure changes progressively from an ordered pyrochlore structure to a disordered defect fluorite structure for $y \geq 0.90$. The disorder process involves, at first, only the O(1) ions that are the nearest neighbors of the vacant anion site. The substituted Zr^{4+} ions replace Ti^{4+} on site B while site A remains occupied only by Y^{3+}. This situation persists until Zr^{4+} has replaced about half of the Ti^{4+} and O(2) has become underoccupied. Replacement of Y^{3+} then begins. Complete randomization of the cation distribution occurs over the relatively narrow composition range $0.60 < y \leq 0.90$. The anion disordering process is thus distinct from that of the cations. A general increase of the anisotropic temperature-factor coefficients occurs as the disorder increases, suggesting a softening of the lattice. The O(1) position, displaced from an ideal cubic array toward the vacant anion site in pyrochlore, relaxes into the ideal position that it would occupy in the fluorite structure, following a quadratic law with y. All of

the partially ordered solid solutions coexist with a small fraction of a fluorite phase in amounts that increased with Zr content. Scattering density maps of the pyrochlore phases for $y = 0.30$ to 0.60 provide no evidence for detectable concentrations of the split-vacancy complex of van Dijk *et al.* (25) in which an interstitial site between a pair of vacant O(1) sites was proposed. Interstitial scattering density occurs at position 8b, a position that corresponds to the missing anion in an ideal fluorite-type structure. The product of O(1) site occupancy and O(1) vacancy concentration provides qualitative explanation of both the magnitude of the change in ion conductivity with increasing disorder and, for $y \geq 0.30$, its dependence on Zr content. This supports the view that fast-ion conduction occurs by O(1) migration among O(1) sites in which vacancy concentrations have been enhanced by displacement of anions to the normally vacant interstitial sites.

ACKNOWLEDGMENTS

We are grateful to Dr. Peter K. Moon for the powder specimens employed in this work, and for discussion with Professor H. L. Tuller. Powder profiles recorded with synchrotron X radiation, analysis of which will be presented elsewhere, were obtained in collaboration with Dr. David Cox at the National Synchrotron Light Source, Brookhaven National Laboratory. This study was performed under support provided by the Sumitomo Metal Mining Corporation and, in part, with the support of Contract DE-FG02-86ER45261 with the Division of Materials Sciences, Office of Basic Energy Research, U.S. Department of Energy.

REFERENCES

1. F. Brisse and O. Knop, *Can. J. Chem.* **45,** 609 (1967).
2. W. E. Klee and G. Weitz, *J. Inorg. Nucl. Chem.* **31,** 2367 (1969).
3. R. A. McCauley, *J. Opt. Soc. Am.* **63,** 721 (1973).
4. B. E. Scheetz and W. B. White, *J. Am. Ceram. Soc.* **62,** 468 (1979).
5. T. van Dijk, R. B. Helmholdt, and A. J. Burggraaf, *Phys. Status Solidi B* **101,** 765 (1980).
6. P. K. Moon, Electrical conductivity and structural disorder in $Gd_2Ti_2O_7$–$Gd_2Zr_2O_7$ and $Y_2Ti_2O_7$–$Y_2Zr_2O_7$ solid solutions, Ph.D. thesis, Massachusetts Institute of Technology, Cambridge, MA, Feb. 1988.
7. M. Oueslati, M. Balkanski, P. K. Moon, and H. L. Tuller, *Mater. Res. Soc. Symp. Proc.* **135,** 199 (1989).
8. A. Rouanet, *Rev. Int. Haute Températures Réfractories* **8,** 161 (1971).
9. M. Perez y Jorba, *Ann. Chim.* **7,** 499 (1962).
10. D. Michel, J. Perez y Jorba, and R. Collongues, *Mater. Res. Bull.* **9,** 1457 (1974).
11. G. Thomas and M. Goringe, "Transmission Electron Microscopy of Materials." Wiley, New York, 1979.
12. S. Suzuki, M. Tanaka, and M. Ishigame, *J. Phys. C Solid State Phys.* **20,** 2963 (1987).
13. T. van Dijk, K. J. de Vries, and A. J. Burggraaf, *Phys. Status Solidi A* **58,** 115 (1980).
14. M. P. van Dijk, K. J. de Vries and A. J. Burggraaf, *Solid State Ionics* **9–10,** 913 (1983).
15. P. K. Moon and H. L. Tuller, *Solid State Ionics* **28–30,** 470 (1988).
16. P. K. Moon and H. L. Tuller, *Mater. Res. Soc. Symp. Proc.* **135,** 149 (1989).
17. M. Spears, S. Kramer, H. L. Tuller, and P. K. Moon, in "Ionic and Mixed Conducting Ceramics" (T. Ramanarayanan and H. L. Tuller, Eds.), p. 32. Proc. 91-12, Electrochemical Society, Pennington, NJ, 1991.
18. C. Heremans, B. J. Wuensch, J. K. Stalick, and E. Prince, *Mater. Res. Soc. Symp. Proc.* **293,** 349 (1993).
19. M. P. Pechini, Method of preparing lead and alkaline earth titanates and niobates and coating method using the same to form a capacitor. U.S. Patent 3,330,697, 1967.
20. M. J. Buergér, *Proc. Nat. Acad. Sci. USA* **42,** 776 (1954).
21. S. M. Haile, B. J. Wuensch, and E. Prince, *Mater. Res. Soc. Symp. Proc.* **166,** 81 (1990).
22. H. M. Rietveld, *J. Appl. Cryst.* **2,** 65 (1971).
23. B. E. Warren, "X-ray Diffraction." Addison–Wesley, Reading, MA, 1969.
24. C. R. A. Catlow, *Solid State Ionics* **53–56,** 955 (1992).
25. M. P. van Dijk, A. J. Burggraaf, A. N. Cormack, and C. R. A. Catlow, *Solid State Ionics* **17,** 159 (1985).